https://doi.org/10.1093/plphys/kiac065 PLANT PHYSIOLOGY 2022: 189: 874–888

Plant Physiology®

Research Article

Rubisco regulation in response to altered carbon status in the cyanobacterium *Synechococcus elongatus* PCC 7942

Amit K. Singh,[1] María Santos-Merino ,[1] Jonathan K. Sakkos ,[1] Berkley J. Walker [1,2] and Daniel C. Ducat [1,3,*,†]

1 MSU-DOE Plant Research Laboratory, Michigan State University, East Lansing, Michigan 48824, USA
2 Department of Plant Biology, Michigan State University, East Lansing, Michigan 48824, USA
3 Department of Biochemistry and Molecular Biology, Michigan State University, East Lansing, Michigan 48824, USA

*Author for correspondence: ducatdan@msu.edu
†Senior author

A.K.S., B.J.W., and D.C.D. conceived the project. A.K.S., M.S.-M., and J.K.S. performed the biological experiments. All authors contributed to data analysis and interpretation. A.K.S. and D.C.D. wrote the article with input and feedback from all authors.
The author responsible for distribution of materials integral to the findings presented in this article in accordance with the policy described in the Instructions for Authors (https://academic.oup.com/plphys/pages/general-instructions) is: Daniel C. Ducat (ducatdan@msu.edu).

Abstract

Photosynthetic organisms possess a variety of mechanisms to achieve balance between absorbed light (source) and the capacity to metabolically utilize or dissipate this energy (sink). While regulatory processes that detect changes in metabolic status/balance are relatively well studied in plants, analogous pathways remain poorly characterized in photosynthetic microbes. Here, we explored systemic changes that result from alterations in carbon availability in the model cyanobacterium *Synechococcus elongatus* PCC 7942 by taking advantage of an engineered strain where influx/efflux of a central carbon metabolite, sucrose, can be regulated experimentally. We observed that induction of a high-flux sucrose export pathway leads to depletion of internal carbon storage pools (glycogen) and concurrent increases in estimates of photosynthetic activity. Further, a proteome-wide analysis and fluorescence reporter-based analysis revealed that upregulated factors following the activation of the metabolic sink are concentrated on ribulose-1,5-bisphosphate carboxylase-oxygenase (Rubisco) and auxiliary modules involved in Rubisco maturation. Carboxysome number and Rubisco activity also increased following engagement of sucrose secretion. Conversely, reversing the flux of sucrose by feeding exogenous sucrose through the heterologous transporter resulted in increased glycogen pools, decreased Rubisco abundance, and carboxysome reorganization. Our data suggest that Rubisco activity and organization are key variables connected to regulatory pathways involved in metabolic balancing in cyanobacteria.

Introduction

Photosynthetic organisms require regulatory mechanisms to overcome dynamic fluctuation in solar illumination, with an ultimate goal of aligning light energy inputs ("source"; i.e. absorbed photonic energy not dissipated by photoprotective mechanisms) with an equivalent capacity to utilize this energy using anabolic metabolism ("sinks"; Bailey and Grossman, 2008; White et al., 2016; Walker et al., 2020). Adaptive responses that poise light-harvesting antennae to a given light quantity/quality are relatively well-described in

Received October 11, 2021. Accepted December 22, 2021. Advance access publication February 24, 2022

cyanobacteria (Grossman et al., 2003; Muramatsu and Hihara, 2012; Montgomery, 2014; Ho et al., 2017). A substantial body of research on cyanobacterial photoprotective processes that dissipate or redistribute excess light excitation is also available (Allahverdiyeva et al., 2013; Mullineaux, 2014; Roach and Krieger-Liszkay, 2014; Kirilovsky and Kerfeld, 2016; Calzadilla and Kirilovsky, 2020; Bhatti et al., 2021). In plants, additional signaling pathways are used to achieve source/sink balance, including signaling networks that monitor key metabolite pools (e.g. sucrose, trehalose-6-phosphate), to poise the expression of photosynthetic machinery, including photosystems (PSs), light-harvesting antennae, and ribulose-1,5-bisphosphate carboxylase-oxygenase (Rubisco; Mccormick et al., 2009; Adams et al., 2013; Lemoine et al., 2013; Sakr et al., 2018; Roth et al., 2019b; Santos-Merino et al., 2021). In contrast to plants, cyanobacteria lack homologs for these signaling functions, making it uncertain how they sense the integrated metabolic demands required for cell homeostasis/growth and coordinate upstream photosynthetic machinery to meet those energetic needs.

A key bottleneck between the light reactions of photosynthesis and downstream central carbon metabolism is Rubisco: a hexadecameric protein complex of large (RbcL) and small (RbcS) subunits that catalyzes the carbon fixation step of the Calvin–Benson–Bassham cycle and is notorious for its low catalytic activity and poor substrate specificity (Spreitzer and Salvucci, 2002; Tcherkez et al., 2006). To overcome Rubisco's enzymatic limitations, cyanobacteria depend upon carbon concentrating mechanisms (CCMs). The cyanobacterial CCM is distinguished by unique features including the carboxysome, a subcellular compartment that greatly enhances the local concentration of CO_2 near Rubisco (Yeates et al., 2008; Borden and Savage, 2021). Structurally, the carboxysome is a protein microcompartment with an outer coat consisting of various protein shell forms (hexamer, pentamer, and trimer), while the inside of the compartment is packed with a paracrystalline-like array of Rubisco organized by the CCM protein M (Cameron et al., 2013; Wang et al., 2019). Plasma membrane-localized bicarbonate transporters actively pump inorganic carbon into the cytosol, which is thought to diffuse through selective carboxysome shell pores, whereupon it is converted into CO_2 by encapsulated carbonic anhydrase (CA). The end result is a concentration of CO_2 around Rubisco up to ~1,000-fold higher than ambient levels (Badger and Price, 2003).

The cyanobacterial CCM is dynamically regulated in response to environmental changes (Raven and Beardall, 2014), a feature that appears to be important for cyanobacterial adaptation to a wide range of ecosystems. Environmental cues (light, CO_2, and temperature) impact bicarbonate transporter gene expression, Rubisco content, and carboxysome composition/morphology (Logothetis et al., 2004; Mackenzie et al., 2004; Sun et al., 2016; Jahn et al., 2018; Rillema et al., 2021). The size and number of carboxysomes are observed to change in response to light quality and quantity (Rohnke et al., 2018; Sun et al., 2019). These changes in carboxysome structure are predicted to impact the relative capacity of the compartment to concentrate CO_2 under different contexts (Mangan and Brenner, 2014). An emerging theory suggests that cyanobacteria regulate the carboxysome to modulate Rubisco activity and optimize cell growth and carbon fixation to environmental conditions. Yet, how CCM regulation is integrated with metabolism and/or changing metabolic demands (e.g. total metabolic flux/load) remains relatively unexplored.

In plants, signaling pathways act to control the activity of Rubisco in response to the downstream metabolic status and to achieve source/sink balance. One well-conserved example involves Hexokinase family members that sense key metabolite pools of carbohydrates. For example, Arabidopsis (*Arabidopsis thaliana*) hexokinase 1 (HXK1) translocates into the nucleus following binding of glucose and forms a complex that suppresses expression of photosynthesis genes including the Rubisco small subunit, chlorophyll *a*/*b* (Chl *a*/Chl *b*) binding proteins of the light-harvesting complex II, and CA (Cho et al., 2006). HXK1 has recently been shown to have conserved roles in the regulation of carbon balance in the microalga *Chromochloris zofingiensis*, and is implicated in a rapid change in the transcriptome of nearly a third of the total genome when cells are fed exogenous sugars, including many genes involved in photosynthesis, Chl *a* biosynthesis, and Rubisco maturation (Roth et al., 2019a).

Recent studies in cyanobacteria support the hypothesis that activation of heterologous metabolic pathways (e.g. engineered bioproduction circuits) can redistribute cellular resources in a manner that requires energetic re-balancing, including that of upstream photosynthetic processes. For example, we have previously shown a notable increase in the relative flux through the photosynthetic electron transport (PET) chain, enhanced CO_2 fixation rates, and reduced acceptor-side limitations on the activity of PSI in the hours following activation of a sucrose-secretion pathway via the expression of proteins sucrose phosphate synthase (SPS) and sucrose permease (CscB) in *Synechococcus elongatus* PCC 7942 (Ducat et al., 2012; Abramson et al., 2016; Santos-Merino et al., 2021). We observed that the upregulation of photosynthetic flux is proportional to the amount of cellular resources that are redirected to the heterologous pathway (Abramson et al., 2016; Santos-Merino et al., 2021); that is, when up to ~80% of photosynthetically fixed carbon is rerouted to the secreted sucrose bioproduct. More widely, a number of other cyanobacterial species and strains engineered to export other carbon metabolites have been shown to experience similar photosynthetic enhancements when heterologous metabolism is engaged, including isobuteraldehyde (Li et al., 2014), 2,3-butanediol (Oliver et al., 2013), and ethylene (Ungerer et al., 2012).

Here, we used modified strains of *S. elongatus* that are capable of sucrose export or import as an approach to experimentally control cyanobacterial sink energy balance. One

such sucrose-exporting strain (*S. elongatus* overexpressing both CscB and SPS; hereafter "CscB/SPS") has been well-characterized for the photosynthetic changes induced by the expression of their heterologous carbon pathway (Ducat et al., 2012; Abramson et al., 2016; Santos-Merino et al., 2021), but longer-term adaptive responses have not been documented. We undertook a systems-level analysis of proteomic changes that accompany engagement of the sucrose "sink," finding that the most significant hits were concentrated around Rubisco and Rubisco-associated factors. Further analysis using live cell imaging and biochemistry shows that carboxysome and Rubisco abundance is dynamically regulated in response to expression of this heterologous sink. Changes observed in sucrose-feeding experiments, whereby exogenous sugars are imported through CscB expression, also support a model linking carboxysome number and organization to metabolic status.

Results

System-level proteomic response to sucrose export

We sought to gain deeper insight into the adaptive cellular response that results from engagement of a strong heterologous carbon sink. We first validated that the previously described CscB/SPS strain (Abramson et al., 2016, 2018; Santos-Merino et al., 2021) was capable of sucrose export under our experimental setup (Figure 1B) and exhibited the previously described changes in photosynthetic parameters upon activation of this heterologous sink via isopropyl β-D-1-thiogalactopyranoside (IPTG) addition (Supplemental Figure S1). We also monitored the internal glycogen content in CscB/SPS 24–48 h following IPTG induction, observing a decline in glycogen stores by >75% on a per-cell basis (Figure 1C). At later time points, glycogen content partially recovers relative to nonsecreting controls (∼30% decrease at 120 h). In other contexts, such as diurnal cycles, glycogen content positively corresponds with cellular carbon abundance (Diamond et al., 2015), suggesting the decrease in glycogen content linked to sucrose export may be a function of increased carbon flux toward the heterologous sucrose export pathway. However, it should be noted that the rate of sucrose efflux is ∼2 orders of magnitude larger than could be accounted for mobilization of glycogen stores alone (Figure 1, B and C).

To expand our analysis of the systemic changes following activation of a heterologous metabolic pathway, we chose an unbiased proteomic approach of CscB/SPS at time intervals 24, 48, 72, and 96 h following induction of sucrose export. We unambiguously identified 913 proteins across all sample conditions and timepoints (Figure 2A), corresponding to a coverage of 34% of total proteins encoded in the genome of *S. elongatus* (913/2,657). Enrichment analysis using Kyoto Encyclopedia of Genes and Genome (KEGG)-assigned gene ontology terms allowed calculation of the percentage enrichment of identified proteins across 17 functional categories relative to the total gene products encoded in the genome (Figure 2B). Across annotated functional categories, >50% proteins within each functional group were identified (Figure 2B). Reduced coverage of lower abundance and/or poorly characterized proteins was observed (240/913 proteins in our proteomics dataset).

Proteomic analysis identified a relatively small set of changes in protein abundance that were consistent across all time points following sucrose export (Figure 2D). CscB and SPS were identified as significantly upregulated in the proteomic analysis, which is expected because they are components specifically induced to trigger sucrose export (Supplemental Table S1). Among the significantly upregulated endogenous proteins (8), the Rubisco enzyme subunits RbcL and RbcS were among the most statistically significant changes (Figure 2C). Further, factors involved in the maturation of Rubisco were also over-represented among the upregulated proteins following sucrose export. This included chaperonins directly associated with the correct folding and assembly of Rubisco into higher order complexes, such as GroEL and its co-factor GroES which contribute to folding of RbcL and assembly of RbcL dimers (Hayer-Hartl et al., 2016). Another upregulated chaperone was high-temperature protein G (Synpcc7942_1813), a member of the heat-shock protein 90A family which plays roles in thermal or oxidative stress response in *Synechococcus* (Hossain and Nakamoto, 2003; Kobayashi et al., 2017). Three additional proteins that were identified as significantly upregulated were iron-deficiency-induced protein A, a factor associated with protection of PSII under various stress conditions (Yousef et al., 2003); Synpcc7942_0369, a conserved but poorly characterized putative oxidoreductase, and; nitrite reductase B, a protein involved in nitrate assimilation and carbon/nitrogen balance (Ohashi et al., 2011; Figure 2C).

The seven proteins that were significantly downregulated following engagement of the sucrose export pathway were not as clearly concentrated around a common molecular function (Supplemental Table S1). Three of the downregulated targets were subunits related to ribosomal activities (Synpcc7942_2020, Synpcc7942_2352, and Synpcc7942_2204; Hood et al., 2016). Two proteins in the antibiotic resistance protein B (AbrB)-like family (Synpcc7942_1969 and Synpcc7942_2255) were downregulated, these have been characterized to act as transcription factors involved in carbon/nitrogen balancing in *Synechocystis* PCC 6803 (Lieman-Hurwitz et al., 2009; Yamauchi et al., 2011; Orf et al., 2016; Rachedi et al., 2020). To better visualize the overall changes in the proteome, we mapped identified proteins with conserved and well-established molecular functions onto a proteomap (Supplemental Figure S2), which can provide a crude approximation of the relative protein abundance of each factor as a function of the summation of identified peptides for each protein (Liebermeister et al., 2014). In addition to the increase in Rubisco subunits, the proteomap highlights a subtle decrease in the abundance of multiple proteins involved in ribosomal functioning and PET chain components (Supplemental Figure S2).

Rubisco is upregulated and reorganized following sucrose export

To independently confirm the proteomic analysis, we evaluated total Rubisco enzyme activity in cell extracts from sucrose exporting cells relative to controls. A significant increase in total Rubisco activity was observed at all time intervals when normalized to Chl *a* content, peaking at ~50% increased activity at 48 h postinduction (Figure 3A). Quantitative Western blots also indicated an increase in Rubisco levels following induction of the sucrose secretion pathway (Figure 3B), this increases similarly in magnitude to the enhanced activity of the in vitro enzyme assay. Increased Rubisco activity is consistent with prior reports that have shown that total carbon fixation rates and total biomass accumulation (i.e. cell biomass plus secreted carbon biomass) increase on a per cell basis when the sucrose secretion pathway is induced (Ducat et al., 2012; Abramson et al., 2016; Santos-Merino et al., 2021).

While we have previously reported enhancements in photosynthetic performance within the hours following induction of the heterologous sucrose sink (Supplemental Figure S1; Ducat et al., 2012; Abramson et al., 2016; Santos-Merino et al., 2021), we do not find comparable evidence for significant alterations in the abundance of the light-harvesting machinery. Consistent with our proteomics dataset (Figure 2C and Supplemental Figure S2), quantitative Western blotting for subunits of key components of the PET chain does not show substantial changes in representative subunits of PSI (PsaC) and PSII (PsbA; Figure 3C).

Effect of exogenous sucrose on photosynthetic activity and glycogen content

One possible interpretation of the physiological changes observed following induction of the sucrose export pathway is that they may be partially related (directly or indirectly) to the depletion of internal pools of carbon and/or energy equivalents. Pathways involved in carbon/energy sensing in plants were classically identified by manipulations that increased or decreased flux of carbon (e.g. sucrose) to specific tissues (Rolland et al., 2006; Lemoine et al., 2013). In order to determine if artificial increases in carbohydrate availability would impact similar cellular features, we examined the effect of supplying exogenous sucrose on cell physiology (Figure 1A). We first analyzed the impact of sucrose feeding on Chl *a* and glycogen content by varying the concentration of sucrose (0–200 mM) with or without inducing expression of the sucrose transporter (CscB). Glycogen content increased by two- to three-fold in cells where external sucrose

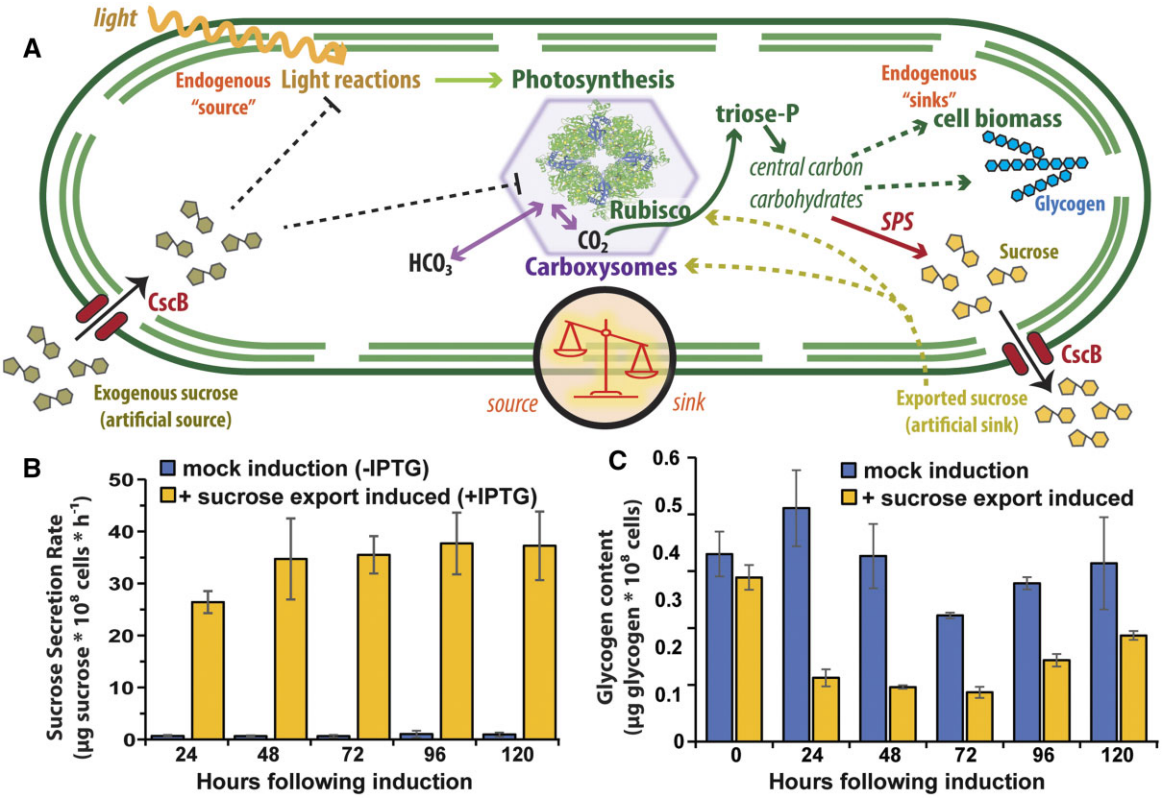

Figure 1 Connection of heterologous sucrose pathway with endogenous metabolism in *S. elongatus*. A, Schematic representation of cyanobacterial source/sink relationships. Endogenous metabolic sinks include metabolism leading to formation of glycogen, sucrose, and other cell biomass are depicted on the right. Cell inputs include light captured for photosynthesis as well as artificially supplied sucrose imported through heterologous transporters. Overexpressed genes for sucrose synthesis (SPS) and transport (CscB) are shown in red. Quantification of exported sucrose (B) and internal glycogen stores (C) for strains induced to express SPS and CscB are shown in time series, with uninduced controls. Error bars represent the SD of three independent biological replicates from the average in a representative time series.

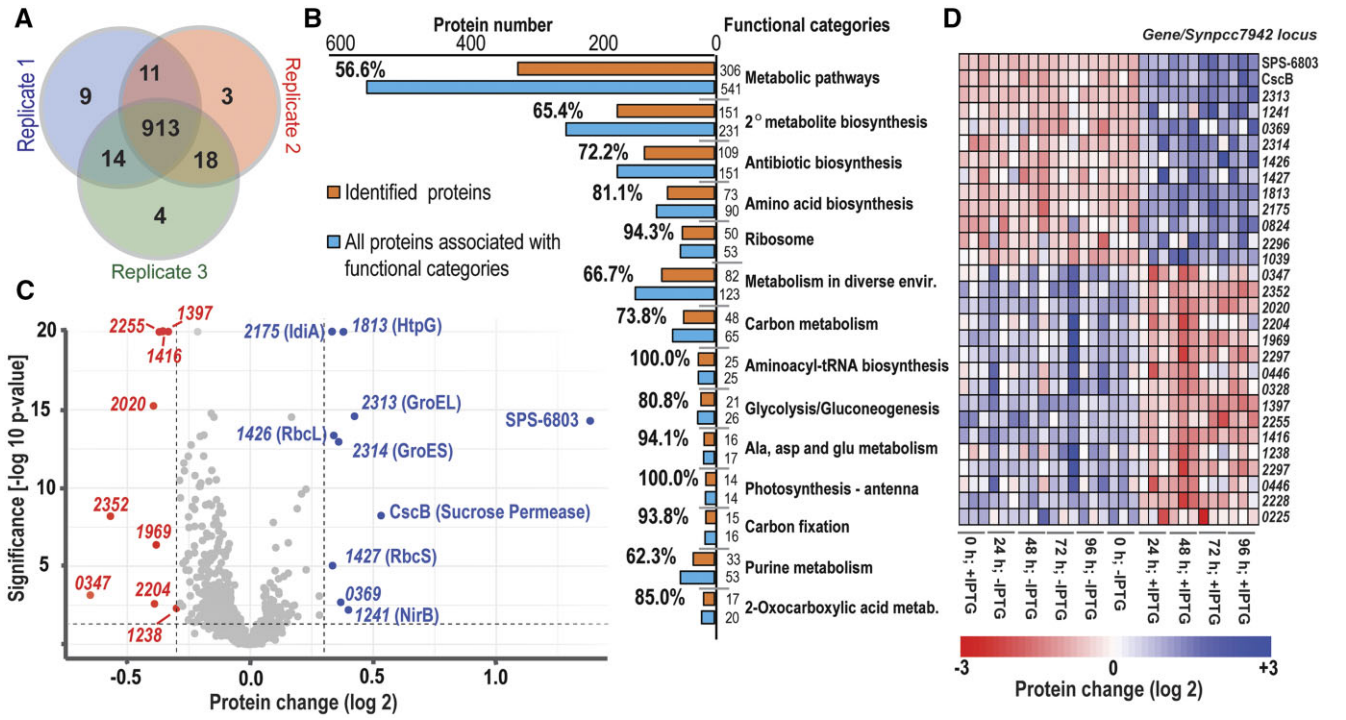

Figure 2 System level proteomic response to sucrose export. A, Venn diagram summarizing the number of unambiguously identified proteins from untargeted proteomic analysis of three biological replicates. B, Representation of proteins from proteomic analysis within established annotated functional groups, with the number and percentage of identified proteins from the indicated categories relative to the total number of proteins with that designation in *S. elongatus* 7942, as assigned by KEGG pathway using the STRING database resource. C, Volcano plot indicating changing protein abundance in induced strains integrated across time points 24, 48, 72, and 96 h relative to controls. The nonaxial vertical dashed-line shows ±0.3 $\log_2$fold protein change and nonaxial horizontal dashed-line shows Mann–Whitney test $P < 0.05$ with Benjamini–Hochberg correction cuttoffs. Differential protein analysis cut-offs were −1.3 > downregulation and + 1.3 < upregulation. Proteins represented by blue data points indicate significantly upregulated proteins, while red points are downregulated. Proteins are identified with the abbreviated number "XXXX" instead of the full genomic locus name (i.e. Synpcc7942_XXXX; Supplemental Table S1). D, Heatmap of significantly upregulated and downregulated proteins for each sample in the proteomic time-series. +

was supplied and CscB was induced to facilitate sucrose uptake in *S. elongatus* (Figure 4A). In the absence of exogenous sucrose (i.e. 0 mM sucrose), inducing expression of CscB did not change glycogen pools. A small, but significant increase in glycogen content was observed at higher exogenous sucrose concentrations (150–200 mM), possibly indicating alternative uptake pathways or indirect effects of the increased osmotic pressure (Page-Sharp et al., 1998; Suzuki et al., 2010).

Cellular Chl *a* content was inversely related to uptake of exogenous carbohydrates, as treatment with 50–200 mM sucrose caused chlorosis only in strains with induced CscB (Figure 4, B and C). As a rise in the total photosynthetic activity (e.g. as measured by evolution of O_2 and assimilation of CO_2) and apparent quantum efficiency of PSII are well-characterized aspects that follow secretion of sucrose (Ducat et al., 2012; Abramson et al., 2016; Santos-Merino et al., 2021) and other carbon products (Oliver et al., 2013), we evaluated the impact of sucrose feeding on photosynthetic parameters. Chl *a* fluorescence-based measurements are routinely used in plants and algae to estimate photosynthetic performance, while cyanobacterial differences (e.g. phycobilin absorbance/fluorescence) require such approaches to be interpreted differently (Campbell et al., 1998; Ogawa et al., 2017). Estimates of PSII activity can be derived as a function of the variable fluorescence in the light (F'_V), which is determined by subtracting the basal fluorescence when the PSII pool is oxidized (F'_0) from the maximal fluorescence (F'_M) when the PSII pool is closed (e.g. under a saturating pulse). Parameters such as the quantum efficiency of PSII (Φ_{II}: [F'_M – Fs/F'_M] see "Materials and methods") and PSII openness (q_P: [(F'_M – Fs)/(F'_M – F'_0)). We observed significantly reduced values in the apparent Φ_{II} and q_P under conditions of sucrose uptake across most measured actinic light intensities (Figure 4, D–F). The reduction in apparent Φ_{II} and q_P was observed regardless of the wavelength of light used to excite the cyanobacterial samples, including conditions that minimized the contribution of phycobilin fluorescence (Supplemental Figure S3).

In tandem with the apparent decrease in Chl *a* fluorescence-based metrics of photosynthetic performance, we independently observed downregulation of components involved in the PET and in the light-harvesting phycobilins. Quantitative Western blot analysis indicated approximately two-fold decrease in the abundance of a core PSII subunit, PsbA, in the presence of 100 mM sucrose when CscB was

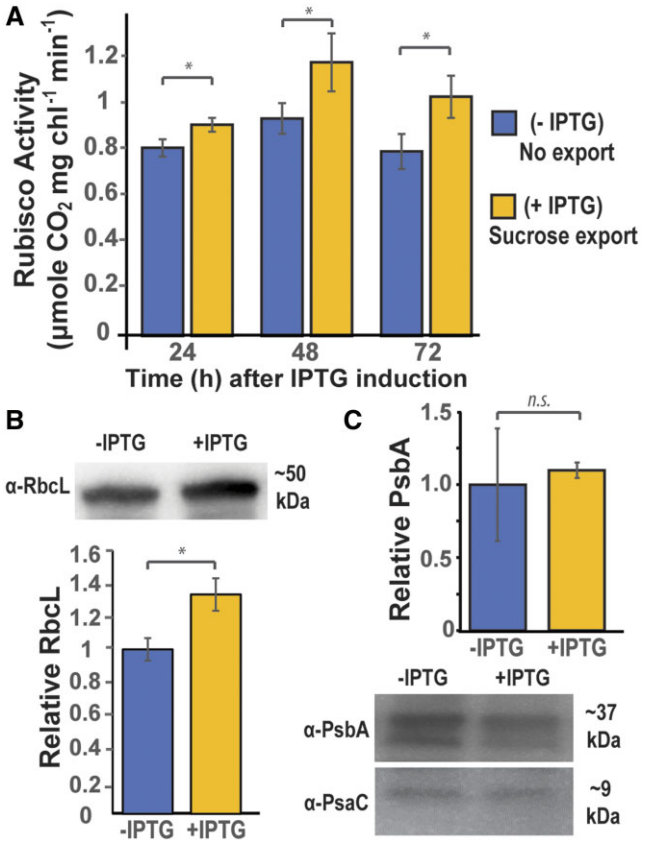

Figure 3 Rubisco is upregulated and reorganized following sucrose export. A, Rubisco activity was measured from CscB/SPS lysates at 24 h intervals following induction of sucrose export (+ IPTG) in comparison to uninduced controls (−IPTG). The activity measured for each sample was normalized to the Chl *a* content of the same sample. Western blots of (B) RbcL (C) PsbA, or PsaC levels were examined 72 h postinduction (+ IPTG) and normalized against uninduced controls (−IPTG). Error bars indicate the SD of three independent biological replicates. Asterisk "*" indicates statistical significance (Student's *t* test, $P < 0.05$) against controls.

expressed (Figure 4E). A central PSI subunit, PsaC, also appeared to be reduced in abundance (Figure 4E; bottom), albeit to a lesser extent than PsbA. Taken together, these results strongly support the interpretation that there is a decrease in total PS abundance in sucrose-importing cells (Figure 4, D–F; Supplemental Figure S3). Phycobilisomes are a major component of light harvesting antennae composed of two phycobiliproteins, allophycocyanin, and phycocyanin. The spectral features of these proteins were reduced by ∼72% and 70% in sucrose-fed cells, respectively (Supplemental Figure S4).

Carboxysomes are reorganized in response to sucrose export and uptake

In cyanobacteria, the bulk of Rubisco is housed within the lumen of the carboxysome. Since we observed changes in Rubisco activity/abundance following sucrose export and import, we examined if the cyanobacterial carboxysome was also altered in response to these interventions. To visualize changes in carboxysome organization, we expressed an exogenous copy of the small subunit of Rubisco fused to the fluorescent reporter mNeonGreen (RbcS-mNG) under the control of the native P_{rbcLS} promoter. Similar constructs have been employed by our group and others to examine carboxysome dynamics in vivo (Savage et al., 2010; Cameron et al., 2013; Chen et al., 2013; Hill et al., 2020). As expected, the RbcS-mNG reporter was concentrated to carboxysomal foci that were arranged along the central axis along the length of the cell when expressed in the mutant background of our strains containing the exogenous *cscB* and/or *sps* genes (Figure 5A and Supplemental Figure S5). Carboxysomes were most frequently arranged in a linear or hexagonal packing that maximizes the distance between neighboring microcompartments (Maccready et al., 2018).

When sucrose export was induced through the heterologous expression of CscB and SPS, we observed changes in carboxysome number and in the intensity of foci (Figure 5, B and C and Supplemental Figure S5). The intensity of RbcS-mNG puncta was noticeably brighter within 24 h of induction of sucrose export, and this difference was maintained for multiple days relative to uninduced controls (Figure 5, B and C). The number of carboxysomes contained within each cell was also increased in the hours following induction of sucrose export (Figure 5, B and C). Since a slight cell elongation and narrowing of cell width was also evident in sucrose-secreting cells (Figure 5A and Supplemental Figure S6), we quantified carboxysome density, observing a slight, but significant increase in carboxysome number relative to cell length in sucrose-exporting cells (Figure 5D). The ratio of cytosolic RbcS-mNG to carboxysome RbcS-mNG remained constant (Supplemental Figure S7). Taken together, this is in agreement with our prior evidence for increased Rubisco content in sucrose-secreting cells (Figures 2 and 3), and suggests that the additional Rubisco remains packaged within carboxysomes, resulting in increased carboxysome number and/or quantity of Rubisco per carboxysome.

When strains containing both the *rbcS-mNG* and *cscB* constructs were fed with exogenous sucrose, we observed changes in carboxysome organization that were tied to sucrose uptake (Figure 6), as well as subtle changes in cell width (Supplemental Figure S8). The number and density of carboxysomes declined in sucrose-importing strains (100 mM sucrose + IPTG; Figure 6A and Supplemental Figures S9 and S10) and there was a change in carboxysome organization (Figure 6A). We observed increased clustering of carboxysome puncta in many cells with the capacity to import exogenous sucrose (Figure 6A (+ IPTG); red arrowheads, Supplemental Figure S9). We also observed an increase in the heterogeneity of puncta size/intensity within each cell, some of this may be attributable to clustering of carboxysomes, but in other cases puncta that appeared to be single carboxysomes at the resolution limits of light microscopy also exhibited notably brighter RbcS-mNG fluorescence relative to puncta within the same cell (Figure 6, A and C; blue arrowheads). Direct assessment of Rubisco protein abundance and activity levels under

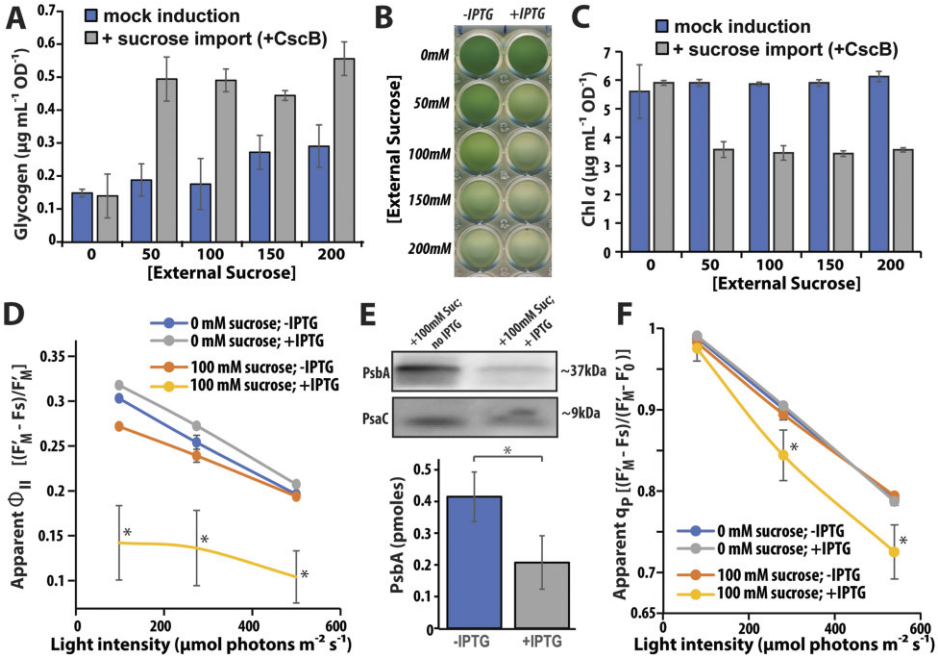

Figure 4 Impact of sucrose uptake on photosynthetic activity and glycogen content. External sucrose was supplemented in growth medium at indicated levels and CscB mutant lines were induced to allow uptake through CscB expression. A, Effect of external sucrose uptake on glycogen content. Measurements of glycogen content were observed under induced (+IPTG) and uninduced (Control; −IPTG) conditions at 24 h time intervals with the indicated levels of externally-supplied sucrose. B, Visual bleaching of CscB strains at 24 h following sucrose uptake. C, Chl *a* content of cultures incubated with external sucrose at 24 h. Photosynthetic parameters such as the apparent PSII quantum yield (Φ_{II}) (D) and estimated fraction of open PSII reaction centers (q_p) (F) were analysed using a custom Chl *a* fluorescence-based spectrometer at actinic light intensities of 100, 275, and 500 µmol photons m^{-2} s^{-1}. E, Western blots of total cellular protein with antibodies targeting PsbA and PsaC from samples in induced and uninduced conditions supplemented with external sucrose. Error bars indicate SD of ⩾3 biological replicates and asterisk "*" shows significant level with $P < 0.05$ by Student's t test (E) and by one-way ANOVA followed by Tukey's multiple comparison test (D and F).

sucrose feeding conditions in the mutant background, a strain containing CscB (but lacking the RbcS-mNG reporter), indicated a ∼25% reduction in Rubisco content on a total protein basis (Figure 6E) and a ∼60% decline in Rubisco activity on a per-cell basis (Figure 6B).

Discussion

Our results suggest that cyanobacteria exhibit numerous changes in photosynthetic components following an engagement of a heterologous sucrose export (sink) pathway, and that these changes are concentrated around Rubisco. We observed changes in the abundance, activity, and organization of Rubisco within carboxysomes after inducing sucrose export, and that many of these effects are reversed when exogenous sucrose is supplied to induce a state of carbon overabundance. Taken together, our evidence suggests that the cyanobacterial CCM—Rubisco and carboxysome organization especially—may respond to internal metabolic signals and source/sink dynamics.

Proteomic changes enhance carbon fixation capacity following engagement of a heterologous carbon sink

We found that a relatively small subset of proteins is significantly altered in response to the activation of our engineered sucrose export pathway. Aside from the expected strong increase in the proteins required for sucrose production (CscB and SPS), four of the remaining eight significantly upregulated proteins were subunits of Rubisco (RbcL and RbcS) or molecular chaperones with established functions in Rubisco's maturation process (GroES and GroEL; Figure 2C). We validated the proteomic results in Rubisco abundance by Western blot (Figure 3B) and Rubisco activity assays (Figure 3A), indicating that adjusted Rubisco levels are a primary target of regulation following engagement of the heterologous sink. Therefore, the increase in total CO_2 fixation and biomass accumulation rates that have been reported following sucrose export (Ducat et al., 2012; Santos-Merino et al., 2021) likely stems both from increased Rubisco catalytic activity and improved efficiency of light reactions of photosynthesis (Abramson et al., 2016; Santos-Merino et al., 2021). Long-term changes in the abundance of other components of photosynthetic machinery (e.g. PSs, light-harvesting complexes, subunits of the PET) following sucrose export are relatively subtle or insignificant by both proteomics approaches and targeted assays (Figures 2 and 3).

We also report alterations in the organization of carboxysomes following sucrose export, as observed by imaging of live cells bearing a fluorescent Rubisco reporter (Figure 5). Despite the observed increase in carboxysome number/

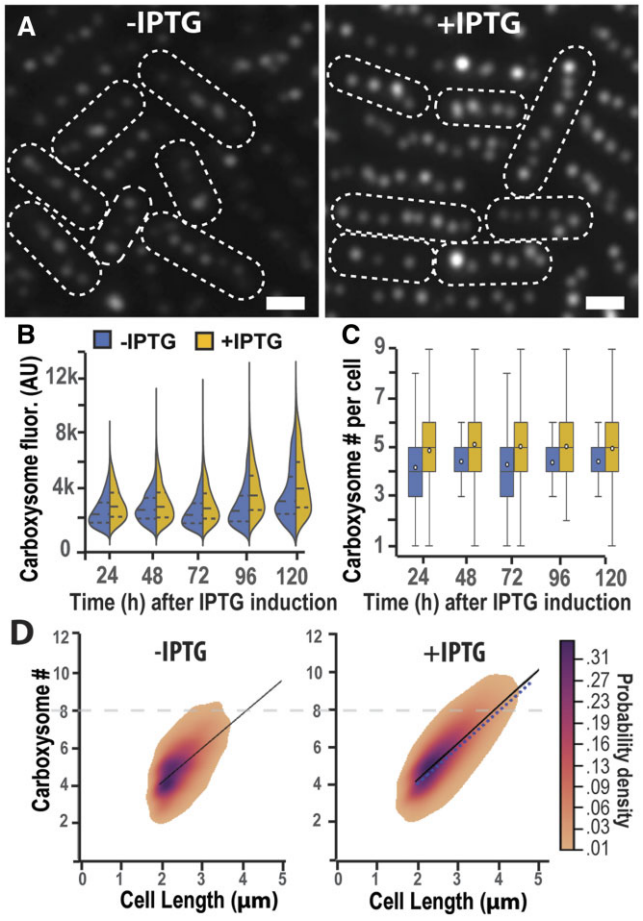

Figure 5 Carboxysomes are reorganized in response to sucrose export. *Synechococcus elongatus* lines bearing a RbcS-mNG reporter were used to visualize carboxysome organization following induction of the sucrose export pathway. A, Representative images of CscB/SPS strains 72 h after sucrose export induction (+IPTG) or control treatment (−IPTG). Violin plots represent the distribution of carboxysome puncta fluorescence intensity (B) and number per cell (C) in induced (+IPTG) cells compared to uninduced controls (−IPTG). D, Density plot of carboxysome number as a function of the containing cell length in both uninduced (−IPTG) and induced (+IPTG) conditions. Probability density is indicated and a linear best-fit trendline is displayed. For visual comparison, a blue dotted trendline of the uninduced sample is overlaid on the induced condition and the gray horizontal dotted line is drawn to facilitate ease of comparison between control and induced populations. Error bars represent ±SD. Each mutant strain has $n > 4{,}000$ cells. Scale bars = 1 μm.

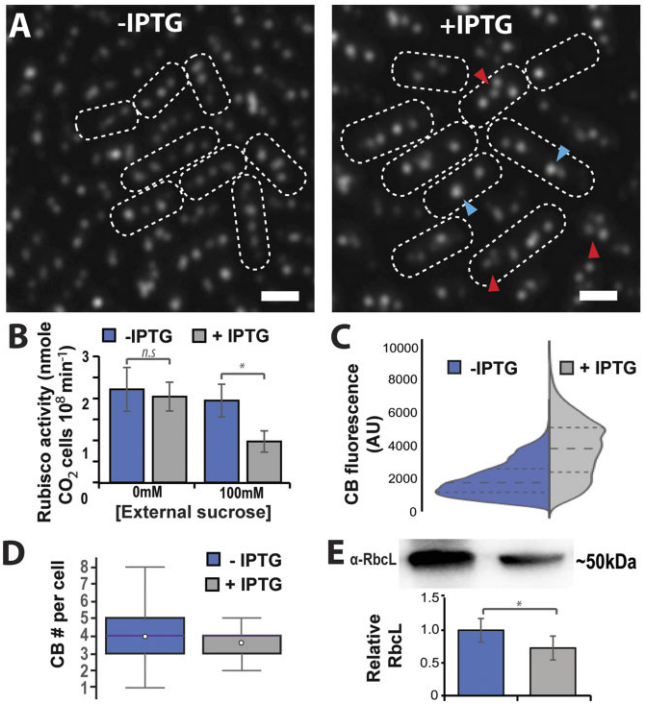

Figure 6 Carboxysomes are reorganized in response to sucrose import. A, Carboxysome reporter (RbcS-mNG) expressed in the CscB strain was visualized following 24 h of incubation in 100 mM external sucrose with the sucrose transporter induced (+IPTG) or without (−IPTG). B, Rubisco activity in strains as above was measured after 24 h of incubation with the indicated external sucrose level. The activity measured for each sample was measured as a function of cell number. Violin and box plots depicting the difference in the distribution of carboxysome puncta intensity (C) and carboxysome number (D) for sucrose importing (+IPTG) strains relative to uninduced. Western blot analysis and relative signal density of Rubisco large subunit (RbcL) abundance in induced and uninduced conditions. E, Each bar represents the mean of three independent biological replicates (±SD). Asterisk "*" shows significant level with $P < 0.05$ by Student's t test. Each analyzed strain has $n > 4{,}000$ cells. AU, Arbitrary units. Scale bars = 1 μm.

density in sucrose-secreting cells (Figure 5, C and D), we did not detect significant upregulation of other carboxysome components in our proteomic analysis (Figure 2C). A simple explanation is that the average size of carboxysomes may be increased in response to sucrose export and that changes in carboxysome surface area (and associated shell/structural proteins) are relatively minor in comparison to the expanded luminal volume and/or change in Rubisco content. Increased carboxysome size would be consistent with the increased carboxysome foci fluorescence intensity we observe in sucrose-secreting cells (RbcS-mNG reporter; Figure 5, B and C). However, we cannot quantify carboxysome size changes due to resolution limits of light microscopy, and other possible interpretations include: 1) shell proteins and other carboxysome structural components increase, but sensitivity limits of proteomics approaches prevent detection (Long et al., 2005; Faulkner et al., 2017); 2) there is no increase in protein level of carboxysome components because they are in excess supply in the cytosol of *S. elongatus* under our growth conditions; 3) carboxysome size remains constant but Rubisco is more densely packaged, or; 4) the RbcS-mNG reporter may not behave identically to native RbcS with regard to luminal packaging.

One hypothesis regarding the physiological changes we observe following engagement of the sucrose secretion pathway is that they are representative of a regulatory response to the altered energy/carbon balance that occurs when a substantial proportion of cellular resources are redirected toward nonnative processes (Santos-Merino et al., 2019). We

and others reported a pronounced decrease in glycogen content in sucrose-secreting cyanobacteria, possibly attributable to the redirection of carbon pools (e.g. glucose and fructose) away from endogenous sinks and to the engineered pathway (Figure 1C; Qiao et al., 2018; Lin et al., 2020). Indirect evidence for this interpretation has also been provided in the form of studies showing that glycogen synthesis is in competition with bioproduct synthesis: reducing the capacity to store cellular carbon as glycogen can improve bioproduction from a number of engineered pathways (Ducat et al., 2012; Davies et al., 2014; Wang et al., 2020). Conversely, heterologous metabolism can mitigate impairments in growth and photosynthesis observed in cyanobacterial strains with restricted flux toward endogenous sinks (Li et al., 2014; Abramson et al., 2016; Xiong et al., 2017; Cano et al., 2018; Díaz-Troya et al., 2020; Santos-Merino et al., 2021).

Rubisco activity and cellular organization are impacted following carbohydrate feeding experiments

If redirection of internal carbon pools away from endogenous metabolism and toward secreted bioproducts results in changes sensed by regulatory machinery in cyanobacteria, it would be expected that interventions that artificially increase internal carbon resources might also result in phenotypic changes in these cellular features. Although *S. elongatus* is regarded as a strict photoautotroph, it can grow photo-mixotrophically when heterologous transporters are expressed (McEwen et al., 2016), a property we used to artificially increase intracellular carbon availability by importing sucrose through the heterologous transporter, CscB. Increased glycogen content and measurements of Chl *a* fluorescence dynamics are consistent with increased cellular carbon resources and an over-reduced PET (Figure 4, A, D, and F and Supplemental Figure S3). Sucrose feeding experiments also result in a rapid downregulation of many components of the photosynthetic machinery, including light-harvesting phycobilisomes, PSs, and Rubisco (Figures 4 and 6). Carboxysome number is decreased, and their spatial positioning is disrupted in sucrose-feeding experiments (compare Figures 5 and 6). One possibility is that metabolic changes that accompany the influx of exogenous carbon impact (directly or indirectly) the activity of maintenance of carboxysome distribution AB proteins (McdA/McdB) involved in microcompartment positioning along the cyanobacterial nucleoid (Maccready et al., 2018). An alternative speculative hypothesis is that exogenous carbohydrate uptake leads to changes in the integrity and/or dynamic association of carboxysome shell proteins on the bacterial microcompartment, as we have recently observed similar phenotypes when we visualize carboxysomes in real-time following destabilization of components of carboxysome shell proteins (specifically, CcmO or CcmL; Sakkos et al., 2021). Distinguishing between these possibilities will require further research with more directed approaches to interrogate carboxysome dynamics and shell integrity. Regardless, our observations raise the possibility that carboxysome properties may be tied to internal metabolic states as well as external environmental conditions (e.g. light, CO_2, and temperature) as previously reported (Woodger et al., 2003; Sun et al., 2016; Rohnke et al., 2018; Sun et al., 2019; Rillema et al., 2021).

Possible implications for source/sink regulatory machinery in cyanobacteria

Rubisco is one of the primary regulatory targets for source/sink regulatory systems in plants (Nielsen et al., 1998; Cho et al., 2006; Granot et al., 2013; Koper et al., 2021). In addition to the previously mentioned mechanistic connection between HXK1 and Rubisco expression, multiple studies in plants have associated intracellular carbohydrate availability with the expression of Rubisco and other components of the photosynthetic machinery. For example, interventions that decrease sink capacity relative to source energy (e.g. exogenous feeding of sugars) lead to decreased Rubisco abundance across many crop plants (Moore et al., 1998; Nielsen et al., 1998; Kasai, 2008; Lobo et al., 2015). Our results suggest that this relationship between Rubisco abundance and source/sink dynamics is maintained in cyanobacteria, although the specific mechanisms for monitoring energetic balance that have been elucidated in plants (e.g. HXK1, SNF-related serine/threonine-protein kinase, and Target of Rapamycin) do not appear to be conserved. This apparent functional conservation may result from the relatively high burden Rubisco synthesis places on photosynthetic organisms (i.e. energetically and in nitrogen requirements). Stated differently, minimizing the cellular burden of Rubisco synthesis in a given environment may be of similar importance to organismal fitness as acquiring sufficient carbon fixation capacity to meet metabolic demands.

A deeper understanding of the mechanisms that regulate source/sink balance in cyanobacteria is likely to have biotechnological implications given the potential for cyanobacteria as a "carbon neutral" production chassis to combat anthropogenic climate change (Sabine et al., 2004; Zhang et al., 2017; DeLisi et al., 2020). Future research is required to determine mechanisms of cyanobacterial source/sink sensing so that they can be leveraged to maximize CO_2 fixation and photosynthetic efficiency in cyanobacteria.

Materials and methods

Growth medium and culture conditions

Cultures of *S. elongatus* PCC 7942 mutant strains were grown in BG-11 (Sigma C3061, Sigma–Aldrich, St. Louis, MO, USA) medium buffered with 1 g L^{-1} 4-(2-hydroxyethyl)-1-piperazineethanesulfonic acid (HEPES), pH 8.3 adjusted with potassium hydroxide. For routine cultivation of cultures, Infors-Multitron incubators with 250 µmol photons m^{-2} s^{-1} compact fluorescent (Sylvania GRO-LUX®, USA) lighting supplemented with 2% (v/v) CO_2 were used at 30°C with orbital shaking at 130 rpm. Cultures were

maintained with a daily back-dilution to OD_{750} ~0.3 unless otherwise noted. The sucrose exporting (CscB/SPS) and importing (CscB) mutants were used as previously described (Abramson et al., 2016). Strains bearing heterologous genes under P_{trc} promoters (i.e. *cscB* and/or *sps*) were induced with 1 mM IPTG as indicated. The carboxysome fluorescence reporter Rubisco small subunit (RbcS-mNG) expression construct was driven by native promoter (P_{rbcLS}) and genomically inserted into Neutral Site (NS1; Clerico et al., 2007). All mutant selections were carried out with BG11 plates with appropriate antibiotic supplementation; Spectinomycin (100 μg mL^{-1}) and Chloramphenicol (25 μg mL^{-1}). Axenic liquid cultures were maintained through supplementation of the same antibiotics, although antibiotics were removed at least 3 d prior to the experiments described.

Total protein extraction and LC–MS/MS analysis

For protein extraction, 50 mL of culture was centrifuged (6,000 × *g*, 15 min, 4°C), supernatants were discarded, and pellets were transferred to 50 mL tubes. All steps of protein extraction were performed at 4°C. The pellets were resuspended in 10 mL of a protein extraction buffer (50 mM Tris–HCl, pH 7.6, 10 mM $MgCl_2$, 0.1% (v/v) TritonX-100, 1X of Halt protease inhibitor cocktail, Thermo Fisher Scientific, Waltham, MA, USA). Cell disruption was performed by French press (AMINCO) at 1,100 psi. After homogenization, the samples were centrifuged (17,000 × *g*, 10 min, 4°C) using round bottom tubes to remove cell debris. The supernatant was transferred to a 50 mL conical tube, and 4 volumes 100% acetone was added, whereupon samples were stored overnight at −20°C for complete protein precipitation. The samples were re-suspended in resuspension buffer (10 mM Tris–HCl, 5% (v/v) SDS, 1% (v/v) β-mercaptoethanol, pH ~8.0) and further used for proteomics measurements using liquid chromatography-mass spectrometry (LC–MS/MS) (for details see Supplemental Method S1).

Raw LC–MS/MS data were further processed for protein identification and differential expression analysis through Scaffold software (version 4.11.1; Proteome Software Inc., Portland, OR, USA). For protein identification, 1% false discovery rate and minimum two unique peptides were specified as cut-offs to filter data for protein identification and analysis. A significance level of $P < 0.05$ (Mann–Whitney test) and Benjamin–Hochberg correction were applied in Scaffold for differential analysis. Enrichment analysis was performed with KEGG pathways assigned functional categories using STRING version 11 database (https://string-db.org). Proteomaps were developed through modification and customization of the online tool (https://www.proteomaps.net/) following user documentation and literature available (Liebermeister et al., 2014).

Fluorescence microscopy and image analysis

For microscopy images, 1 mL of cells were pelleted by centrifugation at 5,000 *g* for 5 min and the pellet was resuspended in 100 μL of BG-11. A 3 μL aliquot was transferred to a 3% (w/v) agarose pad. The cells were allowed to equilibrate for ~5 min before the pad was placed onto a #1.5 glass coverslip for imaging. Fluorescence images were taken with a Zeiss Axio Observer D1 microscope (63x1.3NA) with an Axiocam 503 (mono-chrome) camera using light from X-Cite 120Q (Lumen Dynamics, Mississauga, Canada). For fluorescent mNG signals, we used filter set 46 (000000-1196-681): excitation BP 500/20, emission BP 535/30, and beam splitter FT515. Images were further processed for pixel-based data analysis using MicrobeJ (version 5.12d) an image analysis plugin for ImageJ (Abràmoff et al., 2005; Schindelin et al., 2012). MicrobeJ, as previously reported and described (Ducret et al., 2016), was used to measure carboxysome foci fluorescence and number based on RbcS-mNG reporter fluorescence. The main attributes for defining cell are as follows (Fit shaped; rod shaped; Length: 1.5–10; Width: 0.3–1.5; Area: 1-max) and smoothed maxima foci determination (Tolerance: 100; z-score: 10; Intensity: 0-max). This automated image analysis assisted in removing experimenter bias relative to manual image analysis, however, not all carboxysomes were identified in some instances (e.g. due to low puncta fluorescence or focal plane artifacts).

Rubisco activity assay

Rubisco activity was assayed in vitro spectrophotometrically by following the coupled conversion of reduced Nicotinamide adenine dinucleotide (NADH) to oxidized NAD^+ (Ruuska et al., 1999). For protein extraction, 10 mL of culture was centrifuged (6,000 × *g*, 15 min, 4°C) and supernatant was discarded. The pellets were resuspended in 500 μL of a protein extraction buffer (50 mM *N*-(2-Hydroxyethyl) piperazine-*N*′-(3-propanesulfonic acid, pH 8.1, 1 mM ethylenediaminetetraacetic acid (EDTA), 10 mM dithiothreitol, 0.1% (v/v) TritonX-100, and 1× of Halt protease inhibitor cocktail, Thermo Fisher Scientific, USA) and transferred to 1.5 mL tubes. The cell disruption was performed by sonication (Fisher scientific) using 20 cycles (30 s on: 10 s off) and amplitude 45% at 4°C. After protein extraction, the solution was centrifuged (6,200 × *g*, 10 min, 4°C) to remove cell debris. To fully activate Rubisco, cell-free extracts were incubated at room temperature for 20 min in the presence of 15 mM $NaHCO_3$ and 15 mM $MgCl_2$. Following activation, 40 μL of the lysate was mixed in a cuvette with 960 μL of an assay buffer containing 100 mM HEPES, pH 8.1, 20 mM $MgCl_2$, 1 mM EDTA, 1 mM ATP, 20 mM $NaHCO_3$, 0.2 mM NADH, 30 mM ribulose-1,5-bisphosphate, and a coupling enzyme cocktail containing 20 units (U) glyceraldehyde-3-phosphate dehydrogenase, 22.5 U 3-phosphoglyceric phosphokinase, 12.5 U creatine phosphokinase, 250 U CA, and 56 U triose-phosphate isomerase. The reaction was initiated by adding sample, and the rate of NADH oxidation was monitored at 340 nm for 10 min using a UV spectrometer (Agilent Technologies, Santa Clara, CA, USA). Activity was calculated from the molecular extinction coefficient of NADH. To avoid potential Rubisco inhibitors often found in commercial preparations, RuBP was synthesized and purified in-house and confirmed to have minimal

"fall-over" kinetics on purified Rubisco samples (Kane et al., 1994, 1998).

Biochemical assay for sucrose and glycogen content

Cyanobacterial culture aliquots (2 mL) were pelleted in a centrifuge at 6,200 × *g*. Pellets were processed for the glycogen assay and the supernatant was sampled for sucrose assays. The glycogen assay was performed following the protocol of Nakajima et al. (2017) with modifications. Briefly, pellets were resuspended in 200 µL of 30% (w/v) KOH and incubated in a 95°C in water bath for 2 h. After incubation, 600 µL absolute ethanol was added and further incubated at −20°C overnight. The next day, the suspension was centrifuged and the pellet was dried in an oven. Dried pellets were resuspended in ddH_2O and analyzed with a commercially available Glycogen assay kit (EnzyChrom, San Jose, CA, USA). Sucrose quantification from culture supernatants was determined using the Sucrose/d-Glucose Assay Kit (Megazyme, Bray, Ireland: K-SUCGL) following the manufacturer's instructions.

Pigment analysis

Chl *a* was extracted from cell pellets by incubation in 100% methanol for 30 min at 4°C. Chl *a* was measured spectrophotometrically following the protocols of Porra et al. (1989). Briefly, the pigment suspension was centrifuged and the supernatant was used for absorption at 665 nm. Chl *a* content was determined using an UV/Visible Spectrophotometer (Genesis 20; Thermo, USA). For absorption spectrum and phycobiliprotein content analysis, cells were lysed by glass beads and solubilized phycobilins were recovered in phosphate buffer following the protocol of Zavřel et al. (2018).

Fluorescence measurements of photosynthetic parameters

Estimates of photosynthetic performance in cyanobacteria using Chl *a* fluorescence are not as straightforward as in eukaryotic members of the green lineage, although insights can still be gleaned if appropriate controls and precautions are observed (Campbell et al., 1998; Ogawa et al., 2017). Fluorescence of photosynthetic parameters was measured on a customized fluorimeter/spectrophotometer (Hall et al., 2013) modified for liquid samples. A cuvette with sample was illuminated with a pulsed measuring beam (λ = 590 or 505 nm peak emission light-emitting diode [LED], Luxeon Z Color Line) and then illuminated at three different intensities of photosynthetically active radiation, 100, 275, and 500 µmol photons m^{-2} s^{-1} (λ = 460 nm peak emission, Luxeon Rebel Royal-Blue LED). To acclimate the sample and minimize the impact of successive saturating pulses. the cuvette was illuminated at the relevant actinic light for 3 and 2 min, before the first saturating pulse, and between each pulse, respectively. Cyanobacterial samples containing 2.5 µg mL^{-1} Chl *a* were pelleted, then resuspended in fresh medium sparged with 2% (v/v) CO_2 in air and dark-adapted for 3 min before fluorescence measurements. The relative yields of Chl *a* fluorescence were measured under steady-state illumination (F_s), and 1.5 s saturating pulses were delivered by the LED (~5,000 µmol photons m^{-2} s^{-1}) ($F'm$) and after exposure to ~2 s of darkness with far-red illumination (F'_0). Chl *a* fluorescence was used to calculate apparent values of the quantum yield of PSII (Φ_{II}), and the coefficient of photochemical quenching (q_p) using Equations (1) and (2), respectively (Campbell et al., 1998; Maxwell and Johnson, 2000)

$$\Phi II = \frac{F'm - Fs}{F'm} \quad (1)$$

$$qp = \frac{F'm - Fs}{F'm - F'0}, \quad (2)$$

where F'_m = the value of maximal fluorescence in the light-adapted state, F_s = the steady-state fluorescence in the light-adapted state, and F'_0 = the minimal fluorescence in the light-adapted state.

Western blot analysis

For Western blotting, cells were lysed in extraction buffer (50 mM Tris–HCl, pH 7.6, 10 mM $MgCl_2$, 0.1% (v/v) TritonX-100), fortified with 1× protease inhibitor (Halt protease inhibitor cocktail, Thermo, USA). Extracted protein samples were quantified by using Pierce BCA Protein Assay Kit (Thermo). About 30 µg of total protein extracts was electrophoretically separated on 10% (w/v) SDS-polyacrylamide gels and transferred to a polyvinylidene difluoride membrane preactivated with absolute methanol using Trans-Blot Turbo Transfer System (Bio-Rad Hercules, CA, USA). After blocking with 5% (w/v) powdered skim milk in 1× phosphate buffer solution plus 0.1% (v/v) Tween-20 (PBST), blots were probed with primary antibodies when included, anti-RbcL (PhytoAB, San Francisco, CA, USA; PHY5236A, a dilution of 1:2,000), PsbA (Agrisera, Vännäs, Sweden; AS05084, a dilution of 1:5,000), and PsaC (Agrisera; AS10939, a dilution of 1:5,000) overnight at 4°C. Secondary antibody α-rabbit HRP conjugate (Invitrogen, Waltham, MA, USA; G21234, a dilution of 1:20,000) was incubated with blots for 1 h at room temperature, and antigen–antibody complexes were visualized via a chemiluminescence detection system (Super signal, Thermo scientific, USA). The Precision plus protein dual-color standard (Bio-Rad) was used as reference molecular weight markers.

Statistical analysis

Statistical analysis and plots were generated using Microsoft Excel, R, and python. All experiments were performed with at least three biological replicates and technical replicates for same-day experiments as indicated. Exact replicates and/or *n* values are described in detail in the accompanying figure legends. Statistical tests and indications of statistical significance are also elaborated in figure legends and the main text. Data were shown as mean ± standard deviation (SD). Statistical analysis was performed using one-way analysis of variance (ANOVA) followed by Tukey's multiple comparison test, or Student's test and Mann–Whitney test with

Benjamini–Hochberg correction, when appropriate. Differences were considered statistically significant at $P < 0.05$.

Data availability

The mass spectrometry proteomics data have been deposited to the ProteomeXchange Consortium via the PRIDE (Perez-Riverol et al., 2019) partner repository with the dataset identifier PXD027430 and 10.6019/PXD027430. Proteins were searched against the UniProt protein database UP000002717_*Synehcococcus elongatus* PCC 7942. Rubisco protein structure was downloaded from PDBe-KB and modified for figure display (Figure 1A). The data that support the findings of this study are available from the corresponding author on request.

Accession numbers

Sequence data from this article can be found in the GenBank/EMBL data libraries under accession numbers. *cscB* and *sps* genes were from *Escherichia coli* W genomic DNA (ATCC 9637; ECW_m2594) and *Synechocystis* sp. PCC 6803 (sll0045, SPS-6803), respectively, and used as previously described (Ducat et al., 2012; Abramson et al., 2016).

Supplemental data

The following materials are available in the online version of this article.

Supplemental Figure S1. Photosynthetic activity is enhanced in the sucrose-exporting CscB/SPS mutant of *S. elongatus*.

Supplemental Figure S2. Visualization of cellular protein abundance using proteomaps.

Supplemental Figure S3. Chl *a* fluorescence traces in response to exogenous sucrose supplementation.

Supplemental Figure S4. Pigment profile in sucrose feeding condition.

Supplemental Figure S5. Extended fields of RbcS-mNG in CscB/SPS mutant cells.

Supplemental Figure S6. Comparison of cell size and carboxysome position in sucrose export condition.

Supplemental Figure S7. Comparison of relative fluorescence in sucrose exporting cells.

Supplemental Figure S8. Comparison of cell size and carboxysome position in sucrose feeding experiment.

Supplemental Figure S9. Extended fields of RbcS-mNG in CscB mutant cells.

Supplemental Figure S10. Relationship between carboxysome number and cell length in sucrose import condition.

Supplemental Table S1. List of proteins upregulated and downregulated in sucrose export condition along with overexpressed proteins.

Supplemental Methods. LC–MS-based protein analysis.

Acknowledgments

We would like to thank Dr Curtis G. Wilkerson and Douglas Whitten for mass spectrometry analysis and critical feedback in experimental setup. We would also like to thank Dr. Sigal Lechno-Yossef (Cheryl Lab) and Kaila Smith (Walker Lab) for technical assistance and our laboratory predoctoral fellows Lisa Yun, Emmanuel Kokarakis, and Rees Rillema for helpful comments on this manuscript.

Funding

This work was primarily supported by the Department of Energy and Basic Energy Sciences Division (Grant: DE-FG02-91ER20021). Additional support was provided from the National Science Foundation, Molecular and Cellular Bioscience Division (Grants#: 1845463 and 1517241).

Conflict of interest statement. Authors declare that they have no conflicts of interests.

References

Abràmoff MD, Magalhães PJ, Ram SJ (2005) Image processing with ImageJ Part II. Biophotonics Int **11**: 36–43

Abramson B, Lensmire J, Yang-Tsung L, Jennings E, Ducat D (2018) Redirecting carbon to bioproduction via a growth arrest switch in a sucrose-secreting cyanobacterium. Algal Res **33**: 248–255

Abramson BW, Kachel B, Kramer DM, Ducat DC (2016) Increased photochemical efficiency in cyanobacteria via an engineered sucrose sink. Plant Cell Physiol **57**: 2451–2460

Adams WW, Muller O, Cohu CM, Demmig-Adams B (2013) May photoinhibition be a consequence, rather than a cause, of limited plant productivity? Photosynth Res **117**: 31–44 doi: 10.1007/s11120-013-9849-7

Allahverdiyeva Y, Mustila H, Ermakova M, Bersanini L, Richaud P, Ajlani G, Battchikova N, Cournac L, Aro EM (2013) Flavodiiron proteins Flv1 and Flv3 enable cyanobacterial growth and photosynthesis under fluctuating light. Proc Natl Acad Sci USA **110**: 4111–4116

Badger MR, Price GD (2003) CO_2 concentrating mechanisms in cyanobacteria: molecular components, their diversity and evolution. J Exp Bot **54**: 609–622

Bailey S, Grossman A (2008) Photoprotection in cyanobacteria: Regulation of light harvesting. Photochem Photobiol **84**: 1410–1420

Bhatti AF, Kirilovsky D, van Amerongen H, Wientjes E (2021) State transitions and photosystems spatially resolved in individual cells of the cyanobacterium *Synechococcus elongatus*. Plant Physiol **186**: 569–580

Borden JS, Savage DF (2021) New discoveries expand possibilities for carboxysome engineering. Curr Opin Microbiol **61**: 58–66

Calzadilla PI, Kirilovsky D (2020) Revisiting cyanobacterial state transitions. Photochem Photobiol Sci **19**: 585–603

Cameron JC, Wilson SC, Bernstein SL, Kerfeld CA (2013) Biogenesis of a bacterial organelle: the carboxysome assembly pathway. Cell **155**: 1131–1140 doi: 10.1016/j.cell.2013.10.044

Campbell DA, Hurry V, Clarke A K, Gustafsson P, Oquist G (1998) Chlorophyll fluorescence analysis of cyanobacterial photosynthesis and acclimation. Microbiol Mol Biol Rev **62**: 667–683

Cano M, Holland SC, Artier J, Burnap RL, Ghirardi M, Morgan JA, Yu J (2018) Glycogen synthesis and metabolite overflow contribute to energy balancing in cyanobacteria report glycogen synthesis and metabolite overflow contribute to energy balancing in cyanobacteria. Cell Rep **23**: 667–672

Chen AH, Robinson-Mosher A, Savage DF, Silver PA, Polka JK (2013) The bacterial carbon-fixing organelle is formed by shell envelopment of preassembled cargo. PLoS ONE **8**: e76127 doi: 10.1371/journal.pone.0076127

Cho YH, Yoo SD, Sheen J (2006) Regulatory functions of nuclear hexokinase1 complex in glucose signaling. Cell **127**: 579–589 doi: 10.1016/j.cell.2006.09.028

Clerico EM, Ditty JL, Golden SS (2007) Specialized techniques for site-directed mutagenesis in Cyanobacteria. *In* E Rosato, ed, Circadian Rhythms: Methods and Protocols, Humana Press, Totowa, NJ, pp 155–171

Davies FK, Work VH, Beliaev AS, Posewitz MC (2014) Engineering limonene and bisabolene production in wild type and a glycogen-deficient mutant of *Synechococcus* sp. PCC 7002. Front Bioeng Biotechnol **2**: 1–11

DeLisi C, Patrinos A, MacCracken M, Drell D, Annas G, Arkin A, Church G, Cook-Deegan R, Jacoby H, Lidstrom M, et al. (2020) The role of synthetic biology in atmospheric greenhouse gas reduction: prospects and challenges. BioDesign Res **2020**: 1–8

Diamond S, Jun D, Rubin BE, Golden SS (2015) The circadian oscillator in *Synechococcus elongatus* controls metabolite partitioning during diurnal growth. Proc Natl Acad Sci USA **112**: E1916–E1925

Díaz-Troya S, Roldán M, Mallén-Ponce MJ, Ortega-Martínez P, Florencio FJ (2020) Lethality caused by ADP-glucose accumulation is suppressed by salt-induced carbon flux redirection in cyanobacteria. J Exp Bot **71**: 2005–2017

Ducat DC, Avelar-Rivas JA, Way JC, Silvera PA (2012) Rerouting carbon flux to enhance photosynthetic productivity. Appl Environ Microbiol **78**: 2660–2668

Ducret A, Quardokus EM, Brun YV (2016) MicrobeJ, a tool for high throughput bacterial cell detection and quantitative analysis. Nat Microbiol **1**: 1–7

Faulkner M, Rodriguez-Ramos J, Dykes GF, Owen SV, Casella S, Simpson DM, Beynon RJ, Liu LN (2017) Direct characterization of the native structure and mechanics of cyanobacterial carboxysomes. Nanoscale **9**: 10662–10673

Granot D, David-Schwartz R, Kelly G (2013) Hexose kinases and their role in sugar-sensing and plant development. Front Plant Sci **4**: 44 doi: 10.3389/fpls.2013.00044

Grossman AR, van Waasbergen LG, Kehoe D (2003) Environmental regulation of phycobilisome biosynthesis. In BR Green, WW Parson, eds, Light-Harvesting Antennas in Photosynthesis. Springer Netherlands, Dordrecht, Netherlands, pp 471–493

Hall CC, Cruz J, Wood M, Zegarac R, DeMars D, Carpenter J, Kanazawa A, Kramer D (2013) Photosynthetic measurements with the idea spec: an integrated diode emitter array spectrophotometer/fluorometer. *In* T Kuang, C Lu, L Zhang, eds, Photosynthesis Research for Food, Fuel and the Future, Advanced Topics in Science Technology in China, Springer, Berlin, Heidelberg, pp 184–188

Hayer-Hartl M, Bracher A, Hartl FU (2016) The GroEL-GroES chaperonin machine: A nano-cage for protein folding. Trends Biochem Sci **41**: 62–76 doi: 10.1016/j.tibs.2015.07.009

Hill NC, Tay JW, Altus S, Bortz DM, Cameron JC (2020) Life cycle of a cyanobacterial carboxysome. Sci Adv **6**: eaba1269

Ho M-Y, Soulier NT, Canniffe DP, Shen G, Bryant DA (2017) Light regulation of pigment and photosystem biosynthesis in cyanobacteria. Curr Opin Plant Biol **37**: 24–33

Hood RD, Higgins SA, Flamholz A, Nichols RJ, Savage DF (2016) The stringent response regulates adaptation to darkness in the cyanobacterium *Synechococcus elongatus*. Proc Natl Acad Sci USA **113**: E4867–E4876

Hossain M, Nakamoto H (2003) Role for the cyanobacterial HtpG in protection from oxidative stress. Curr Microbiol **46**: 70–76

Jahn M, Vialas V, Karlsen J, Maddalo G, Edfors F, Forsström B, Uhlén M, Käll L, Hudson EP (2018) Growth of cyanobacteria is constrained by the abundance of light and carbon assimilation proteins. Cell Rep **25**: 478–486.e8 doi: 10.1016/j.celrep.2018.09.040

Kane HJ, Viil J, Entsch B, Paul K, Morrell MK, Andrews TJ (1994) An improved method for measuring the CO_2/O_2 specificity of ribulosebisphosphatte carboxylase-oxygenase. Aust J Plant Physiol **21**: 449–461

Kane HJ, Wilkin JM, Portis AR Jr, John Andrews T (1998) Potent inhibition of ribulose-bisphosphate carboxylase by an oxidized impurity in ribulose-1,5-bisphosphate1. Plant Physiol **117**: 1059–1069

Kasai M (2008) Regulation of leaf photosynthetic rate correlating with leaf carbohydrate status and activation state of Rubisco under a variety of photosynthetic source/sink balances. Physiol Plant **134**: 216–226

Kirilovsky D, Kerfeld CA (2016) Cyanobacterial photoprotection by the orange carotenoid protein. Nat Plants **2**: 16180

Kobayashi I, Watanabe S, Kanesaki Y, Shimada T, Yoshikawa H, Tanaka K (2017) Conserved two-component Hik34-Rre1 module directly activates heat-stress inducible transcription of major chaperone and other genes in *Synechococcus elongatus* PCC 7942. Mol Microbiol **104**: 260–277

Koper K, Hwang SK, Singh S, Okita TW (2021) Source–sink relationships and its effect on plant productivity: Manipulation of primary carbon and starch metabolism. *In* BK Sarmah, BK Borah, eds, Genome Engineering for Crop Improvement, Springer International Publishing, Cham, Switzerland, pp 1–31

Lemoine R, La Camera S, Atanassova R, Dédaldéchamp F, Allario T, Pourtau N, Bonnemain JL, Laloi M, Coutos-Thévenot P, Maurousset L, et al. (2013) Source-to-sink transport of sugar and regulation by environmental factors. Front Plant Sci **4**: 272 doi: 10.3389/fpls.2013.00272

Li X, Shen CR, Liao JC (2014) Isobutanol production as an alternative metabolic sink to rescue the growth deficiency of the glycogen mutant of *Synechococcus elongatus* PCC 7942. Photosynth Res **120**: 301–310 doi: 10.1007/s11120-014-9987-6

Liebermeister W, Noor E, Flamholz A, Davidi D, Bernhardt J, Milo R (2014) Visual account of protein investment in cellular functions. Proc Natl Acad Sci USA **111**: 8488–8493

Lieman-Hurwitz J, Haimovich M, Shalev-Malul G, Ishii A, Hihara Y, Gaathon A, Lebendiker M, Kaplan A (2009) A cyanobacterial AbrB-like protein affects the apparent photosynthetic affinity for CO_2 by modulating low-CO_2-induced gene expression. Environ Microbiol **11**: 927–936

Lin PC, Zhang F, Pakrasi HB (2020) Enhanced production of sucrose in the fast-growing cyanobacterium *Synechococcus elongatus* UTEX 2973. Sci Rep **10**: 390 doi: 10.1038/s41598-019-57319-5

Lobo AKM, de Oliveira Martins M, Lima Neto MC, Machado EC, Ribeiro RV, Silveira JAG (2015) Exogenous sucrose supply changes sugar metabolism and reduces photosynthesis of sugarcane through the down-regulation of Rubisco abundance and activity. J Plant Physiol **179**: 113–121 doi: 10.1016/j.jplph.2015.03.007

Logothetis K, Dakanali S, Ioannidis N, Kotzabasis K (2004) The impact of high CO_2 concentrations on the structure and function of the photosynthetic apparatus and the role of polyamines. J Plant Physiol **161**: 715–724 doi: 10.1078/0176-1617-00942

Long BM, Price GD, Badger MR (2005) Proteomic assessment of an established technique for carboxysome enrichment from *Synechococcus* PCC7942. Can J Bot **83**: 746–757

Maccready JS, Hakim P, Young EJ, Hu L, Liu J, Osteryoung KW, Vecchiarelli AG, Ducat DC (2018) Protein gradients on the nucleoid position the carbon-fixing organelles of cyanobacteria. Elife **7**: e39723 doi: 10.7554/eLife.39723

Mackenzie TDB, Burns RA, Campbell DA, Brunswick N, Brunswick N (2004) Carbon status constrains light acclimation in the cyanobacterium. **136**: 3301–3312

Mangan N, Brenner M (2014) Systems analysis of the CO_2 concentrating mechanism in cyanobacteria. Elife **3**: e02043 doi: 10.7554/eLife.02043

Maxwell K, Johnson GN (2000) Chlorophyll fluorescence—a practical guide. J Exp Bot **51**: 659–668

Mccormick AJ, Watt DA, Cramer MD (2009) Supply and demand: sink regulation of sugar accumulation in sugarcane. J Exp Bot **60**: 357–364

McEwen JT, Kanno M, Atsumi S (2016) 2,3-Butanediol production in an obligate photoautotrophic cyanobacterium in dark

conditions via diverse sugar consumption. Metab Eng **36**: 28–36 doi: 10.1016/j.ymben.2016.03.004

Montgomery BL (2014) The regulation of light sensing and light-harvesting impacts the use of cyanobacteria as biotechnology platforms. Front Bioeng Biotechnol **2**: 22 doi: 10.3389/fbioe.2014.00022

Moore BD, Cheng SH, Rice J, Seemann JR (1998) Sucrose cycling, Rubisco expression, and prediction of photosynthetic acclimation to elevated atmospheric CO_2. Plant Cell Environ **21**: 905–915

Mullineaux CW (2014) Electron transport and light-harvesting switches in cyanobacteria. Front Plant Sci **5**: 7

Muramatsu M, Hihara Y (2012) Acclimation to high-light conditions in cyanobacteria: From gene expression to physiological responses. J Plant Res **125**: 11–39

Nakajima T, Yoshikawa K, Toya Y, Matsuda F, Shimizu H (2017) Metabolic flux analysis of the synechocystis sp. PCC 6803 ΔnrtABCD mutant reveals a mechanism for metabolic adaptation to nitrogen-limited aonditions. Plant Cell Physiol **58**: 537–545

Nielsen TH, Krapp A, Röper-Schwarz U, Stitt M (1998) The sugar-mediated regulation of genes encoding the small subunit of Rubisco and the regulatory subunit of ADP glucose pyrophosphorylase is modified by phosphate and nitrogen. Plant Cell Environ **21**: 443–454

Ogawa T, Misumi M, Sonoike K (2017) Estimation of photosynthesis in cyanobacteria by pulse-amplitude modulation chlorophyll fluorescence: problems and solutions. Photosynth Res **133**: 63–73

Ohashi Y, Shi W, Takatani N, Aichi M, Maeda SI, Watanabe S, Yoshikawa H, Omata T (2011) Regulation of nitrate assimilation in cyanobacteria. J Exp Bot **62**: 1411–1424

Oliver JWK, Machado IMP, Yoneda H, Atsumi S (2013) Cyanobacterial conversion of carbon dioxide to 2,3-butanediol. Proc Natl Acad Sci USA **110**: 1249–1254 doi: 10.1073/pnas.1213024110

Orf I, Schwarz D, Kaplan A, Kopka J, Hess WR, Hagemann M, Klähn S (2016) CyAbrB2 contributes to the transcriptional regulation of low CO2 acclimation in synechocystis sp. PCC 6803. Plant Cell Physiol **57**: 2232–2243

Page-Sharp M, Behm CA, Smith GD (1998) Cyanophycin and glycogen synthesis in a cyanobacterial *Scytonema* species in response to salt stress. FEMS Microbiol Lett **160**: 11–15

Perez-Riverol Y, Csordas A, Bai J, Bernal-Llinares M, Hewapathirana S, Kundu DJ, Inuganti A, Griss J, Mayer G, Eisenacher M, et al. (2019) The PRIDE database and related tools and resources in 2019: Improving support for quantification data. Nucleic Acids Res **47**: D442–D450

Porra RJ, Thompson WA, Kriedemann PE (1989) Determination of accurate extinction coefficients and simultaneous equations for assaying chlorophylls a and b extracted with four different solvents: Verification of the concentration of chlorophyll standards by atomic absorption spectroscopy. Biochim Biophys Acta **975**: 384–394

Qiao C, Duan Y, Zhang M, Hagemann M, Luo Q, Lu X (2018) Effects of reduced and enhanced glycogen pools on salt-induced sucrose production in a sucrose-secreting strain of *Synechococcus elongatus* PCC 7942. Appl Environ Microbiol **84**: 1–11

Rachedi R, Foglino M, Latifi A (2020) Stress signaling in cyanobacteria: A mechanistic overview. Life **10**: 312 doi: 10.3390/life10120312

Raven JA, Beardall J (2014) CO_2 concentrating mechanisms and environmental change. Aquat Bot **18**: 24–37 doi: 10.1016/j.aquabot.2014.05.008

Rillema R, Hoang Y, MacCready JS, Vecchiarelli AG (2021) Carboxysome mispositioning alters growth, morphology, and rubisco level of the cyanobacterium *Synechococcus elongatus* PCC 7942. MBio **12**: e02696-20

Roach T, Krieger-Liszkay A (2014) Regulation of photosynthetic electron transport and photoinhibition. Curr Protein Pept Sci **15**: 351–362

Rohnke BA, Singh SP, Pattanaik B, Montgomery BL (2018) RcaE-dependent regulation of carboxysome structural proteins has a central role in environmental determination of carboxysome morphology and abundance in Fremyella diplosiphon. mSphere **3**: e00617-17, doi: 10.1128/msphere.00617-17

Rolland F, Baena-Gonzalez E, Sheen J (2006) SUGAR SENSING AND SIGNALING IN PLANTS: Conserved and novel mechanisms. Annu Rev Plant Biol **57**: 675–709 doi: 10.1146/annurev.arplant.57.032905.105441

Roth MS, Gallaher SD, Westcott DJ, Iwai M, Louie KB, Mueller M, Walter A, Foflonker F, Bowen BP, Ataii NN, et al. (2019a) Regulation of oxygenic photosynthesis during trophic transitions in the green alga *Chromochloris zofingiensis*. Plant Cell **31**: 579–601 doi: 10.1105/tpc.18.00742

Roth MS, Westcott DJ, Iwai M, Niyogi KK (2019b) Hexokinase is necessary for glucose-mediated photosynthesis repression and lipid accumulation in a green alga. Commun Biol **2**: 347 doi: 10.1038/s42003-019-0577-1

Ruuska S, Andrews TJ, Badger MR, Hudson GS, Laisk A, Price GD, von Caemmerer S (1999) Interplay between limiting processes in C3 photosynthesis studied by rapid-response gas exchange using transgenic tobacco impaired in photosynthesis. Funct Plant Biol **25**: 859–870

Sabine CL, Feely RA, Gruber N, Key RM, Lee K, Bullister JL, Wanninkhof R, Wong CS, Wallace DWR, Tilbrook B, et al. (2004) The oceanic sink for anthropogenic CO_2. Science **305**: 367–371 doi: 10.1126/science.1097403

Sakkos JK, Hernandez-Ortiz S, Osteryoung KW, Ducat DC (2021) Orthogonal degron system for controlled protein degradation in cyanobacteria. ACS Synth Biol **10**: 1667–1681

Sakr S, Wang M, Dédaldéchamp F, Perez-Garcia M-D, Ogé L, Hamama L, Atanassova R (2018) Molecular sciences the sugar-signaling hub: Overview of regulators and interaction with the hormonal and metabolic network. Int J Mol Sci **19**: 2506 doi: 10.3390/ijms19092506

Santos-Merino M, Singh AK, Ducat DC (2019) New applications of synthetic biology tools for cyanobacterial metabolic engineering. Front Bioeng Biotechnol **7**: 33 doi: 10.3389/fbioe.2019.00033

Santos-Merino M, Torrado A, Davis GA, Rottig A, Bibby TS, Kramer DM, Ducat DC (2021) Improved photosynthetic capacity and photosystem I oxidation via heterologous metabolism engineering in cyanobacteria. Proc Natl Acad Sci USA **118**: e2021523118 doi: 10.1073/pnas.2021523118

Savage DF, Afonso B, Chen AH, Silver PA (2010) Spatially ordered dynamics of the bacterial carbon fixation machinery. Science **327**: 1258–1261

Schindelin J, Arganda-Carreras I, Frise E, Kaynig V, Longair M, Pietzsch T, Preibisch S, Rueden C, Saalfeld S, Schmid B, et al. (2012) Fiji: an open-source platform for biological-image analysis. Nat Methods **9**: 676–682

Spreitzer RJ, Salvucci ME (2002) R UBISCO: Structure, regulatory interactions, and possibilities for a better enzyme. Annu Rev Plant Biol **53**: 449–475 doi: 10.1146/annurev.arplant.53.100301.135233

Sun Y, Casella S, Fang Y, Huang F, Faulkner M, Barrett S, Liu LNN (2016) Light modulates the biosynthesis and organization of cyanobacterial carbon fixation machinery through photosynthetic electron flow. Plant Physiol **171**: 530–541

Sun Y, Wollman AJM, Huang F, Leake MC, Liu LN (2019) Single-organelle quantification reveals stoichiometric and structural variability of carboxysomes dependent on the environment. Plant Cell **31**: 1648–1664

Suzuki E, Ohkawa H, Moriya K, Matsubara T, Nagaike Y, Iwasaki I, Fujiwara S, Tsuzuki M, Nakamura Y (2010) Carbohydrate metabolism in mutants of the cyanobacterium *synechococcus elongatus* PCC 7942 defective in glycogen synthesis. Appl Environ Microbiol **76**: 3153–3159

Tcherkez GGB, Farquhar GD, Andrews TJ (2006) Despite slow catalysis and confused substrate specificity, all ribulose bisphosphate

carboxylases may be nearly perfectly optimized. Proc Natl Acad Sci USA **103**: 7246–7251

Ungerer J, Tao L, Davis M, Ghirardi M, Maness PC, Yu J (2012) Sustained photosynthetic conversion of CO2 to ethylene in recombinant cyanobacterium Synechocystis 6803. Energy Environ Sci **5**: 8998–9006

Walker BJ, Kramer DM, Fisher N, Fu X (2020) Flexibility in the energy balancing network of photosynthesis enables safe operation under changing environmental conditions. Plants **9**: 301 doi: 10.3390/plants9030301

Wang H, Yan X, Aigner H, Bracher A, Nguyen ND, Hee WY, Long BM, Price GD, Hartl FU, Hayer-Hartl M (2019) Rubisco condensate formation by CcmM in β-carboxysome biogenesis. Nature **566**: 131–135 doi: 10.1038/s41586-019-0880-5

Wang M, Luan G, Lu X (2020) Engineering ethanol production in a marine cyanobacterium Synechococcus sp. PCC7002 through simultaneously removing glycogen synthesis genes and introducing ethanolgenic cassettes. J Biotechnol **317**: 1–4

White AC, Rogers A, Rees M, Osborne CP (2016) How can we make plants grow faster? A source-sink perspective on growth rate. J Exp Bot **67**: 31–45

Woodger FJ, Badger MR, Price GD (2003) Inorganic carbon limitation induces transcripts encoding components of the CO_2-concentrating mechanism in *Synechococcus* sp. PCC7942 through a redox-independent pathway. Plant Physiol **133**: 2069–2080

Xiong W, Cano M, Wang B, Douchi D, Yu J (2017) The plasticity of cyanobacterial carbon metabolism. Curr Opin Chem Biol **41**: 12–19

Yamauchi Y, Kaniya Y, Kaneko Y, Hihara Y (2011) Physiological roles of the cyAbrB transcriptional regulator pair Sll0822 and Sll0359 in synechocystis sp. strain PCC 6803. J Bacteriol **193**: 3702–3709

Yeates TO, Kerfeld CA, Heinhorst S, Cannon GC, Shively JM (2008) Protein-based organelles in bacteria: carboxysomes and related microcompartments. Nat Rev Microbiol **6**: 681–691 doi: 10.1038/nrmicro1913

Yousef N, Pistorius EK, Michel KP (2003) Comparative analysis of idiA and isiA transcription under iron starvation and oxidative stress in *Synechococcus elongatus* PCC 7942 wild-type and selected mutants. Arch Microbiol **180**: 471–483

Zavřel T, Chmelík D, Sinetova MA, Červený J (2018) Spectrophotometric determination of phycobiliprotein content in cyanobacterium synechocystis. J Vis Exp **2018**: 1–9

Zhang A, Carroll AL, Atsumi S (2017) Carbon recycling by cyanobacteria: Improving CO_2 fixation through chemical production. FEMS Microbiol Lett **364**: 1–7